Synthesis of Activated Carbon-Fe_3O_4 Composite as Gasoline Adsorbent in Gasoline-Water Mixture and Its Adsorption Kinetics Study

Monica Niken Aprilliani
Department of Chemistry, Faculty of Mathematics and Natural Sciences, Universitas Gadjah Mada

Rusdiarso, Bambang
Department of Chemistry, Faculty of Mathematics and Natural Sciences, Universitas Gadjah Mada

Trisunaryanti, Wega
Department of Chemistry, Faculty of Mathematics and Natural Sciences, Universitas Gadjah Mada

https://doi.org/10.5109/4843101

出版情報：Evergreen. 9 (3), pp.701-710, 2022-09. 九州大学グリーンテクノロジー研究教育センター
バージョン：

Synthesis of Activated Carbon-Fe_3O_4 Composite as Gasoline Adsorbent in Gasoline-Water Mixture and Its Adsorption Kinetics Study

Monica Niken Aprilliani, Bambang Rusdiarso, Wega Trisunaryanti*

Department of Chemistry, Faculty of Mathematics and Natural Sciences, Universitas Gadjah Mada, Sekip Utara, Yogyakarta 55281, Indonesia

*Author to whom correspondence should be addressed:
E-mail: wegats@ugm.ac.id

(Received May 31, 2022; Revised September 4, 2022; accepted September 20, 2022).

Abstract: Activated carbon-Fe_3O_4 composite was successfully synthesized. This work aimed to synthesize magnetic activated carbon and study its performance as a gasoline adsorbent. Dried coconut shells were pyrolyzed using a microwave to produce activated carbon (AC). The activated carbon-Fe_3O_4 composite was synthesized by the co-precipitation method, resulting in AC-M. Contact angles of AC-M with three different kinds of liquid were calculated using Drop Analysis LB-ADSA plugin in the ImageJ application program. Contact angles between AC-M with water, gasoline-water mixture, and gasoline were 84.156 ˚, 72.928 ˚, and 0 ˚, respectively. The contact angles show the hydrophobic properties of the composite. The adsorption capacity of AC-M for gasoline adsorption was 1252.22 mg/g for adsorption time 4 min and mass of adsorbent 0.09 g and followed the adsorption kinetic pseudo-second-order model from Ho and McKay with adsorption rate constant 0.0012 g/mg/min.

Keywords: activated carbon-Fe_3O_4 composite; coconut shell activated carbon; contact angle; gasoline adsorbent; magnetic adsorbent

1. Introduction

One of the causes of polluted waters is oil spills resulting from leaks during oil exploration and transportation[1-2]. Oil spills can lead to water surfaces covered with oil and inhibit sunlight and oxygen entering the aquatic ecosystem. It can worsen because the oil layer on the water surface will spread due to the waves and wind[2]. One of the highly efficient methods to remove oil spills is adsorption using various adsorbent materials[3]. Adsorption is widely used to extract crude oil spills because of its simple application, low energy required, relatively low cost, and produce no by-products[1-6]. Different materials have been prepared as adsorbents of different kinds of oil, including crude oil[3-4]. However, the conventional adsorption method has a limitation, in which the recollection of used adsorbents from water is too time-consuming. Magnetic adsorbents can be easily collected using an external magnetic field[1, 6]; therefore, several works to prepare magnetic adsorbents of crude oil have been done[5, 7].

Raj and Joy[5] have synthesized a composite of activated carbon based on coconut shells and Fe_3O_4 nanoparticles by *in situ* coprecipitation technique for crude oil adsorption. The success of the synthesis of the activated charcoal-Fe_3O_4 composite can be identified from FTIR and XRD analysis[5, 8-9]. Activated carbon gives adsorbent properties to this composite and is commonly used as an adsorbent in separation systems and purification systems. The adsorption capacity of activated carbon is related to its porosity, surface area, pore volume, and pore size distribution[10]. Activated carbon can be used as a selective adsorbent for organic compounds. This property is influenced by oxygen-containing functional groups (OCFG) presence on the surface of activated carbon, escalating the surface's hydrophobic property[11].

Activated carbon can be prepared from carbon-rich biomass by the carbonization step and the activation step[12]. Kurniati *et al.*[13] have synthesized activation carbon from coconut shell pyrolyzed at 400 ˚C, chemically activated followed by physically activated at 400 ˚C for 2.5 h. In their work, Raj and Joy[5] have prepared activated carbon from coconut shell pyrolyzed at a high temperature of 1000 ˚C, followed by physical activation at 1000 ˚C. The impurities in the form of tar and volatile material should be removed to obtain carbon. The removal of impurities takes place at high temperatures, up to 600-1000 ˚C[14]. The high temperature and long time required in conventional pyrolysis make the procedure economically inefficient. Microwave-assisted pyrolysis (MAP) can be used as an alternative method since this method can lower the reaction temperature; hence the

energy required is also reduced[15-16].

The material used as oil adsorbent must have high selectivity towards oil than water and high oil adsorption capacity. Then, it is expected to have hydrophobic properties. The hydrophobicity of a material can be described by the large water contact angle formed by the material with a drop of liquid[17-18]. Relatively hydrophobic material shows a water contact angle close to 90 ˚ or above, while relatively hydrophilic material forms a less than 90 ˚ contact angle with water[17]. Besides water, the contact angle can be measured between material and various kinds of liquid. The smaller contact angle between solid material and liquid implies that the material has a stronger affinity towards the liquid, following the "like dissolve like" principle[18]. One of the easiest computerized methods to measure contact angle is the Low Bond Axisymmetric Drop Shape Analysis (LB-ADSA) plugin from the ImageJ application program[19].

In this work, activated carbon-Fe_3O_4 composite was synthesized, and its performance as gasoline adsorbents was investigated. Activated carbon based on coconut shells was prepared by the MAP method. Activated carbon-Fe_3O_4 composite was synthesized by the co-precipitation method. The contact angles between the composite and three different kinds of liquid, including water, gasoline, and gasoline-water mixture, were measured using the LB-ADSA plugin from the ImageJ application program. The adsorption activity of activated carbon-Fe_3O_4 composite for gasoline adsorption from the water surface was investigated by evaluating the influence of adsorption time and mass of adsorbent used to adsorption capacity. The adsorption kinetics models to study the adsorbent's performance used in this work were pseudo-first-order, pseudo-second-order, and intra-particle diffusion adsorption kinetics models.

2. Experimental

2.1 Materials

The local traditional market in Magelang supplied the dried coconut shell. The analytical grades $FeCl_3.6H_2O$ and $FeCl_2.4H_2O$ were purchased from Merck. Concentrated ammonia solution and distilled water were purchased from a local supplier. Retail gasoline from PT. Pertamina was used to examine the adsorbent performance of adsorbing gasoline.

2.2 Instrumentation

The microwave oven was used to pyrolyze coconut shells in the activated carbon preparation. The functional groups of activated carbon, composite, and used adsorbent were analyzed by Prestige-21, Shimadzu FT-IR spectrometer with a data station in the range of 400-4000 cm^{-1}. XRD analysis was carried out using Philips Xpert Powder Diffractometer with Cu Kα monochromatized radiation source, operated at 40 kV, 30 mA, at a scan rate of 4 ˚/min between 3-90 ˚. The surface morphology was captured by Hitachi Flexem 1000, and EDAX Ametek analyzed elemental composition. Quantachrome Novatouch Lx4 carried out pore size and surface area analysis. The degassing was processed at 300 ˚C. N_2 adsorption-desorption isotherm was measured by the multipoint BET method. BET method was used to measure the specific surface area. BJH desorption model was used to provide mesoporous size distribution. The hydrocarbon composition of commercial gasoline was identified by GC2010 MSQP 2010S Shimadzu.

2.3 Procedure

2.3.1 Preparation of activation carbon

The coconut shell was cleaned with soap and water, then cut into smaller pieces. After that, the coconut shell was dried at 100 ˚C for 24 h. The dried coconut shell was crushed into powder and sifted. The coconut shell powder was then pyrolyzed with a microwave oven at 800 W for 10 min. The activated carbon obtained was cooled at room temperature and coded AC.

2.3.2 Synthesis of activated carbon-Fe_3O_4 composite

The synthesis of activated carbon-Fe_3O_4 composite was done by a similar procedure done by Raj and Joy[5]. The mixture of 2.92 g of $FeCl_3.6H_2O$, 1.074 g of $FeCl_2.4H_2O$, 0.5 g of prepared AC, and 15 mL of distilled water was stirred while heated to 80 ˚C, and concentrated ammonia solution was added by dripping until pH 12. The precipitate formed was left in the mother liquor for one hour and was filtered using filter paper. The black powder was rinsed with distilled water to neutral pH and was dried at 100 ˚C. The resulting product was coded AC-M.

2.3.3 Contact angles measurements

The contact angle formed between the adsorbent surface and liquid can be measured by a computerized method. In this work, the contact angles were measured using Low Bond Axisymmetric Drop Shape Analysis (LB-ADSA) plugin from the ImageJ program. The plugin detects the edges of the drop image by finding the points with a contrasting gradient. The result of this analysis will be optimum if the image has a good black and white contrast. The LB-ADSA plugin uses five variables to make a green Young-Laplace drop shape that is superimposed upon the drop image[19].

Some AC-M was placed on a sheet of white paper covered by a plastic sheet. The surface of AC-M was fattened. A drop of water was placed onto the surface, then the image of the droplet was captured. The image capturing was done at room temperature and pressure. The droplet image was edited to grayscale using the ImageJ application program. The contact angle between water and the solid surface was measured by drop analysis LB-ADSA plugin from the ImageJ application program. The same procedure also measured contact angles between the AC-M surface and the gasoline and gasoline-water

mixture. The gasoline-water mixture (BA) was made by mixing 10 mL of distilled water and 2 g of gasoline. The mixture was stirred using a magnetic stirrer until gasoline dots spread evenly in the water.

2.3.4 Determination of adsorption capacity

The gasoline, water, and gasoline adsorption capacity from the gasoline-water mixture (BA) using AC-M were measured according to the following procedure. 2 g of gasoline was inserted into the beaker glass, and a fixed amount of AC-M was added for a specific adsorption time. AC-M with adsorbed gasoline was retaken using a magnet bar covered by an aluminum foil sheet of known mass. The total mass of aluminum foil, AC-M, and adsorbed gasoline was weighted. A similar procedure was carried out to measure water adsorption capacity. To examine the adsorption capacity of gasoline from the BA mixture, the artificial oil spill on the water surface was made. 10 mL of distilled water was inserted into a beaker glass, and then 2 g of gasoline was added to its surface without further treatment. After that, the same procedure as gasoline and water adsorption capacity examination was conducted. This examination was performed using variations in the adsorption times (1, 2, 3, 4, 5, 10, and 10 min) and variations in the ratio of the adsorbent to adsorbate (6:200; 7:200; 8:200; 9:200; 10:200; 11:200; and 12:200).

The adsorption capacity, q_t (mg/g) is the ratio of the mass of adsorbed adsorbate at time t (m_t, mg) and the mass of adsorbent used (m_0, g)[7]. Meanwhile, q_e is adsorption capacity in equilibrium. The adsorption capacity can be calculated by Eq. (1)[7].

$$q_t = \frac{m_t}{m_0} \tag{1}$$

2.3.5 Adsorption kinetics study

Three adsorption kinetics models were used to investigate the adsorption mechanism of gasoline from BA. The three models were the pseudo-first-order model from Lagergren, the pseudo-second-order model from Ho and McKay, and the intra-particle diffusion from Weber-Morris. The adsorption rate constant of pseudo-first-order (k_1) can be obtained by the graphic plot of $\log(q_e - q_t)$ vs. t[20]. The pseudo-first-order (PFO) kinetic equation can be represented by the following Eq. 2[21]:

$$\log(q_e - q_t) = \log(q_e) - \frac{k_1}{2.303} t \tag{2}$$

where q_t (mg/g) and q_e (mg/g) are adsorption capacity at time t (min) and equilibrium, respectively, while k_1 (min^{-1}) is the PFO rate constant.

The pseudo-second order (PSO) model is related to the vacant active sites, and the chemisorption process is the rate-controlling[6, 20, 22]. The PSO kinetic equation is expressed by Eq. 3[6, 20, 22]:

$$\frac{t}{q_t} = \frac{1}{k_2 {q_e}^2} + \frac{1}{q_e} t \tag{3}$$

where k_2 (g/mg/min) is the PSO rate constant and can be determined by the graphic plot of t/q_t vs. t.

The intra-particle diffusion (IPD) model was utilized to investigate the mass transport mechanism and rate-limiting step of kinetics[7, 20]. The IPD model is expressed by following Eq. 4[20, 22]:

$$q_t = k_{id} t^{1/2} + C \tag{4}$$

where k_{id} ($mg/g/min^{0.5}$) is the intra-particle diffusion rate constant, and C (mg/g) is the intercept. The thickness between the adsorbent and adsorbate is depicted by the intercept of equation[6, 22]. The value of k_{id} can be determined by the graphic plot of q_t vs. $t^{1/2}$.

3. Result and Discussion

3.1 Material Characterization

3.1.1 Functional groups analysis

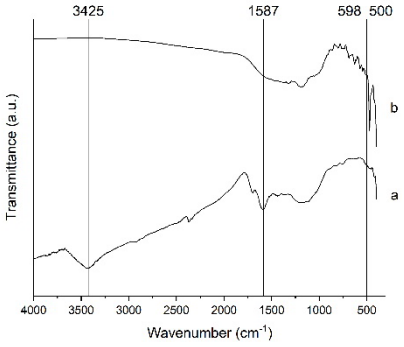

Fig. 1: FT-IR spectra of (a) activated carbon (AC) and (b) activated carbon-Fe_3O_4 composite (AC-M)

The difference in FT-IR spectra of AC and AC-M showed in Fig. 1. FT-IR spectra of AC show no peaks in the 500-610 cm^{-1} region. On the other hand, AC-M showed two peaks at 500 and 598 cm^{-1}. These peaks correspond to Fe—O vibrations in Fe_3O_4 nanocrystals[4, 6]. In pure Fe_3O_4 FT-IR spectra, these peaks are seen in wavenumber 585 and 632 cm^{-1}. The shifting of these peaks to the lower energy region indicates the activated carbon surface has successfully bonded with Fe_3O_4 nanoparticles[5].

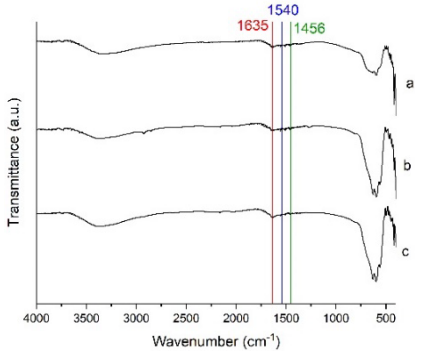

Fig. 2: FT-IR spectra of (a) activated carbon-Fe_3O_4 composite (AC-M), (b) AC-M after being used to adsorb pure gasoline (AC-M') and (c) gasoline from BA (AC-M").

Table 1. FTIR spectra peak list of AC, AC-M, AC-M', and AC-M"

AA		AA-M		AA-M'		AA-M"	
1161	C-O	500	Fe-O	492	Fe-O	492	Fe-O
1587	C=C	598	Fe-O	594	Fe-O	598	Fe-O
3425	O-H stretching	1456	C-H bending	1506	O-H bending		
		1506	O-H bending	1540	C=O	1634	C=O
		1540	C=C	1558	C=O	3364	O-H stretching
		1635	C=O	3361	O-H stretching		
		3335	O-H stretching				

After being used as a gasoline adsorbent, the changes in functional groups in AC-M were observed using FT-IR spectroscopy. The FT-IR spectra of used AC-M, coded AC-M' and AC-M", showed in Fig. 2. Several peaks from AC-M did not show in both AC-M' and AC-M". The peak at 1456 cm^{-1}, indicating C-H bending vibration did not appear in AC-M' and AC-M". The peak at 1635 cm^{-1}, indicating C=O stretching on the carboxylate anion, was also not detected in AC-M' spectra. Moreover, the peak at 1540 cm^{-1} that shows C=C stretching vibration was not detected in AC-M" spectra. The disappearance of these peaks can be caused by the bonding form process between the surface of AC-M and the component of gasoline.

3.1.2 XRD analysis

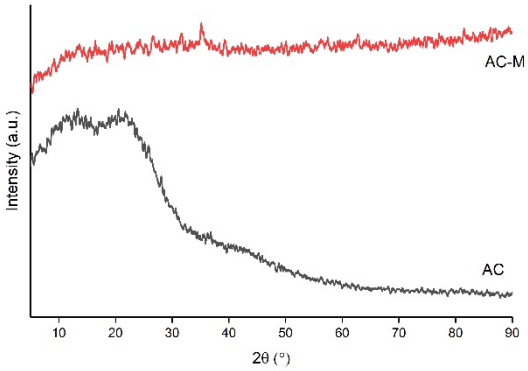

Fig. 3: XRD pattern of AC and AC-M

XRD analysis was done for AC and AC-M to observe the diffraction pattern changes when AC was being used to synthesize AC-M. The diffractogram of AC and AC-M are shown in Fig. 3. The diffractogram of AC shows three broad peaks at around 2θ = 13.34 °, 20.51 °, and 43.55 °. The broad peaks indicate that AC is an amorphous solid and has no crystallography structure and pattern. After AC-M was formed, the diffraction pattern changes, and new peaks are formed. The diffraction pattern of AC-M was then analyzed by GSAS II software[23] and compared with the Fe_3O_4 diffraction pattern reference standard. The reference standard is based on the research by Wechsler B A, et al[24]. Fig. 4 shows the refinement curve between the observation curve and calculation curve.

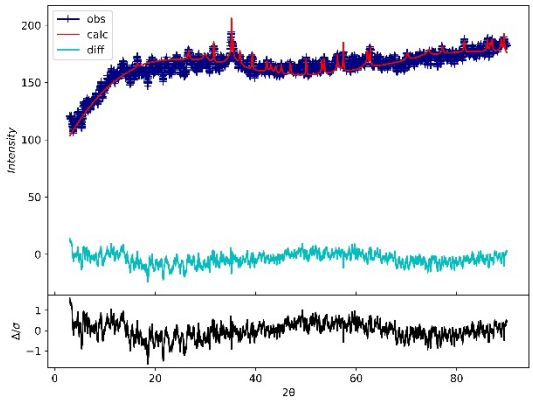

Fig. 4: Refinement curve between the observation curve of AC-M and the calculation curve of Fe_3O_4 reference standard by means of GSAS

Fig. 4 shows the refinement curve between the observation curve and the calculation curve. The observation curve is the diffraction pattern of AC-M obtained by XRD analysis. On the other hand, the calculation curve is the calculated curve by the reference. The green curve is the difference curve. The normalized error distribution curve only leaves the background peaks (the black curve) from the sample measurement. The fitting of the observation curve and calculation curve is showing a good level of fit despite the intensity of the observation curve being lower than the calculation curve. The lower intensity of the peaks in the AC-M diffraction pattern is due to the lower percentage of Fe_3O_4 in AC-M that is being combined with activated carbon than the pure Fe_3O_4 from the reference. The same reason leads to the AC-M diffraction pattern looks like full of noise. The amorphous properties of activated carbon are combined with the crystalline properties of magnetite, hence lowering the peaks of the magnetite diffraction pattern.

3.1.3 Morphology and elemental surface analysis

The surface morphology of AC-M was analyzed using an SEM instrument. The SEM image of AC-M with a magnification of 1000× (as shown in Fig. 5a) indicates that AC-M particles are varied in shape and size. From the SEM image of AC-M, the pores can be seen at its surface. The surface elemental of AC-M was analyzed using an EDX instrument combined with an SEM instrument. EDX spectrum as shown in Fig. 5b suggests that AC-M is composed of O, Fe, and C as the main elements. C atoms are from the activated carbon, Fe atoms are from Fe_3O_4, and O atoms are from both. The main component of AC-M is Fe, with a mass percentage of 65.51 %, followed by O and C with a mass percentage of 25.37 and 8.41 %, respectively. In SEM-EDX the surface elemental is analyzed by shooting the sample surface with electron beams and collecting the released energy as x-ray with unique energy for each element. Hence, the result only describes the surface elemental of a certain area of the sample. A high mass percentage of Fe found is due to the

uneven distribution of Fe on the sample surface. Besides the main elements, a small amount of Si with a mass percentage of 0.71 % was also found in AC-M. Si is one of the most found impurities in activated carbon synthesized from waste carbon sources and is a contaminant from its surrounding.

The porous structure of AC-M is caused by the activated carbon structure, and it contributes to its adsorbent properties. The Fe content of AC-M signifies the presence of magnetite. It makes AC-M has a magnetic property and can be attracted to a magnetic field.

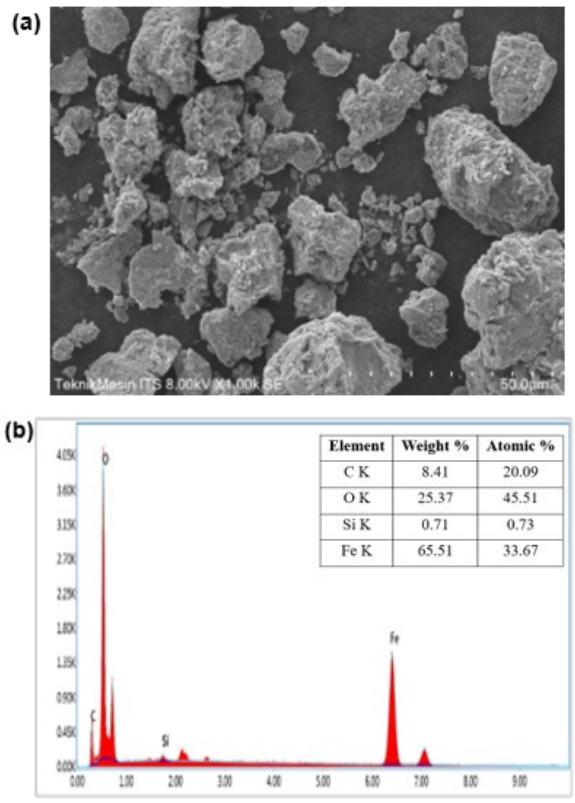

Fig. 5: (a) SEM image and (b) elemental surface composition of AC-M

3.1.4 Surface area and pore size analysis

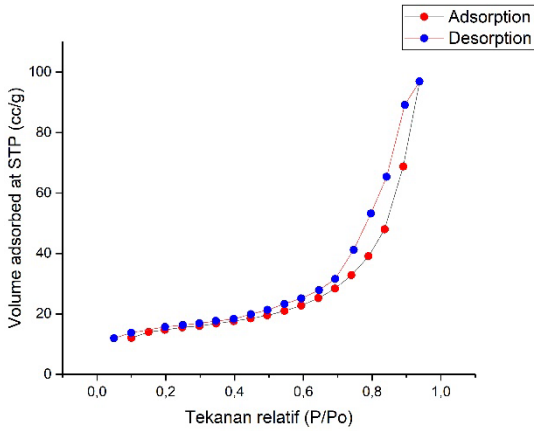

Fig. 6: N_2 adsorption-desorption isotherm profile of AC-M

The adsorbent properties of AC-M are influenced by its surface area and pore size properties[22, 25]. The surface area of AC-M was studied by N_2 adsorption-desorption isotherm analysis at 77.35 K. AC-M showed the adsorption-desorption type IVa according to IUPAC classification types as shown in Fig. 6. This type of isotherm is a characteristic of mesoporous adsorbents. The adsorption behavior of the mesoporous materials is affected by the interactions that occur among the adsorbent and adsorptive, and also by the interaction between the adsorbate molecules[26]. In type IVa isotherm, capillary condensation is composed of hysteresis and occurs when the pore width exceeds a certain critical width that depends on the adsorption system and temperature[27].

The specific surface area was measured by the multipoint BET method. The analysis result shows that the BET specific surface area of AC-M is 55.202 m^2/g. The high surface area makes AC-M could be used as a promising gasoline adsorbent. The total pore volume of AC-M was 0.150 cc/g for pores with radii less than 16.43 nm. The average pore size was measured by the BJH desorption model. The analysis result shows that AC-M has an average pore radius of 5.443 nm.

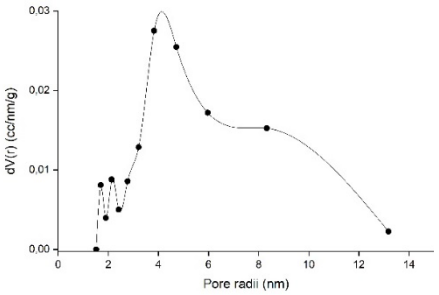

Fig. 7: Pore size distribution of AC-M shows that the average radius of AC-M is around 5 nm

The pore size distribution of AC-M was made by the desorption BJH analysis data to investigate the uniformity of the pore sizes of AC-M, assuming the pore shape is cylindrical. The pore size distribution is the total pore volume for any pore radius. Fig. 7 shows the wide graph indicating that AC-M has pores of various sizes with an average radius of around 5 nm. The results show that AC-M is a mesoporous material. Mesoporous materials are known for their properties as an adsorbent. If the pore radius of the adsorbent is too small, the diffusion of adsorbates and solvents will be limited and enhances the shielding effect for larger molecules.

3.1.5 Magnetic properties analysis

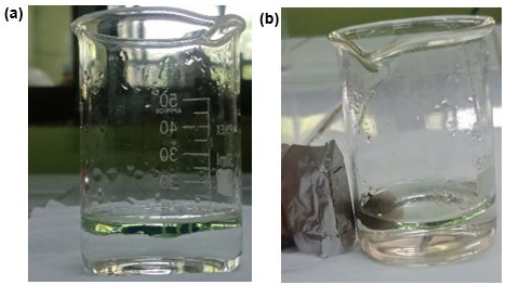

Fig. 8: (a) AC-M on the gasoline layer and (b) AC-M was pulled to the magnetic bar proof their magnetism property

Magnetism is one of the most important properties to make the adsorbent could be retaken easily from the waters[1,5,6,7]. The magnetic property was tested qualitatively using an external magnetic bar. AC-M powder was carefully placed on the gasoline layer in the artificial oil spills on water. An external magnetic bar was brought closer to the vessel. AC-M was pulled to the magnetic bar, as shown in Fig. 8, indicating the magnetic property of the composite.

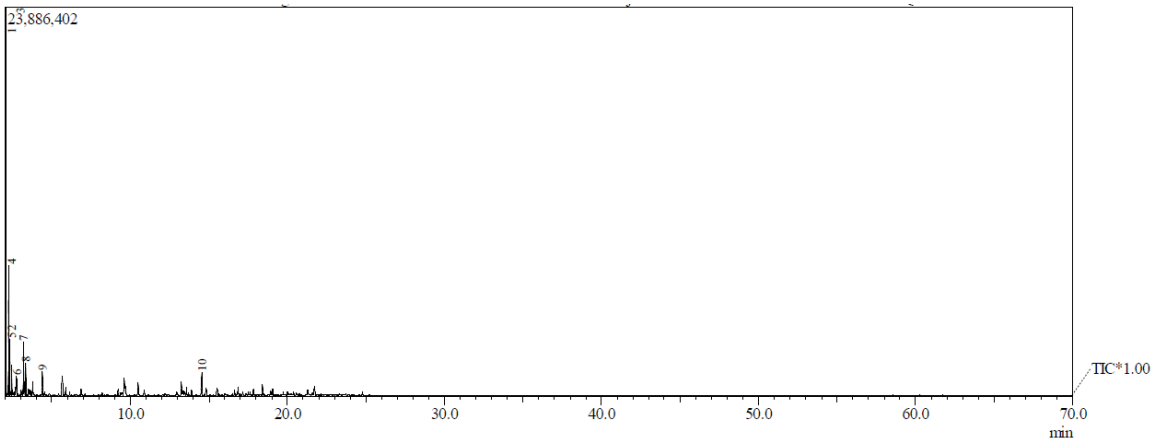

Fig. 9: Chromatogram of commercial gasoline from PT. Pertamina (Pertalite)

3.2 Hydrophobicity of the Activated carbon-Fe_3O_4 Composite

3.2.1 GC-MS analysis of commercial gasoline

The gasoline used for adsorption performance examination in this work is commercial gasoline from PT. Pertamina, with a commercial name of Pertalite. The gasoline was analyzed by GC-MS instrument to find out the hydrocarbon composition of the gasoline. The chromatogram shows that gasoline is composed of various hydrocarbon compounds indicated by various retention times, as shown in Fig. 9. The retention time describes the amount of time needed for a compound to get through the column and reach the detector. The Y-axis describes the intensity, which is a reflection of the amount of specific compound that is present in the sample. The highest peak indicates the component with the highest percentage present in the sample. Table 2 shows the mass spectrometry data based on its m/z ratio and compared it with the library. The mass spectra showed that gasoline is composed of several kinds of hydrocarbon, with 5 to 12 carbon atoms, including paraffin, olefin, and aromatic hydrocarbons. 2,2-dimethyl butane is the most abundant component with a percentage of 26.99 %. This makes the gasoline has non-polar property. To efficiently adsorb the gasoline, the adsorbent must also have a non-polar property. This property can be described by the hydrophobicity of the adsorbent from the measurement of its contact angle with water, gasoline, and BA mixture[17)]

Table 2. Hydrocarbon composition of commercial gasoline Pertalite identified by mass spectra library

No.	Compound	Formula	Molecular mass	Retention time	Area (%)
1.	2-methyl butane	C_5H_{12}	72	1.869	26.99
2.	n-pentane	C_5H_{12}	72	1.936	6.00
3.	2,2-dimethyl butane	C_6H_{14}	86	2.075	28.84
4.	2,3-dimethyl butane	C_6H_{14}	86	2.234	12.57
5.	3-methyl pentane	C_6H_{16}	86	2.333	4.50
6.	2-methyl-1-pentene	C_6H_{12}	84	2.743	2.81
7.	4-methyl-1-pentene	C_6H_{12}	84	3.190	6.61
8.	n-heptane	C_7H_{16}	100	3.338	3.83
9.	Methylcyclohexane	C_7H_{14}	98	4.398	3.41
10.	1,2,4-trimethylbenzene	C_9H_{12}	120	14.547	4.44

3.2.2 Contact angles measurement

AC-M as a gasoline adsorbent must have a hydrophobic property. This property can be depicted by the contact angles between AC-M and three kinds of fluid, including water, gasoline, and BA. AC-M formed a more significant angle with water than with BA; at the same time, AC-M did not form an angle with gasoline, as shown in Fig. 10. The contact angles formed with water, BA, and gasoline were 84.156 ˚, 72.928 ˚, and 0 ˚, respectively. From this result, it can be concluded that AC-M has a significant affinity toward gasoline, and the water contact angle close to 90 ˚ indicates AC-M is macroscopically hydrophobic[18)].

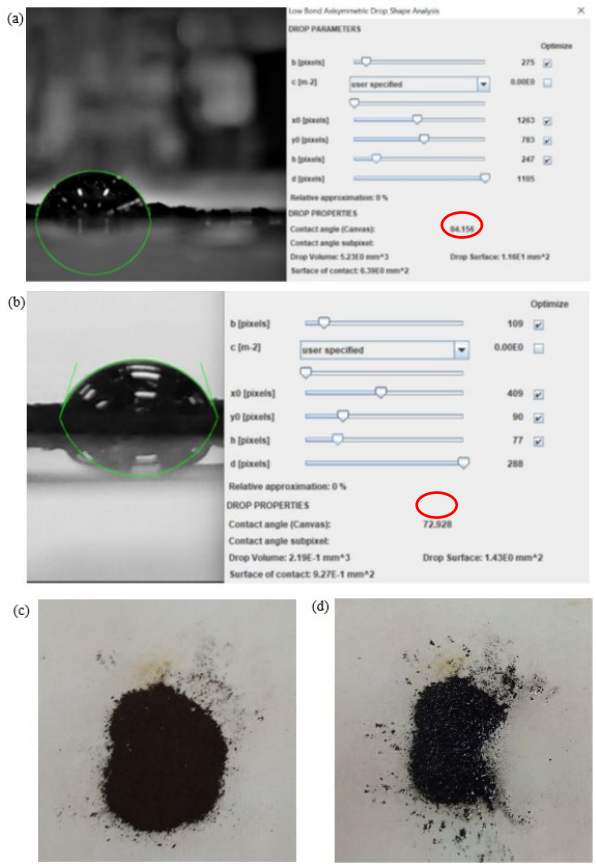

Fig. 10: The contact angles of AC-M with (a) water, (b) BA, and (c) AC-M before being dripped with gasoline, and (d) AC-M after being dripped with gasoline. The contact angle from the largest to the smallest are the water, BA, and gasoline contact angle

3.3 Activated carbon-Fe_3O_4 Composite Performance As Gasoline Adsorbent

3.3.1 Time influences

Adsorption time is a factor that influences adsorption capacity and it determines the effectiveness of the use of the material as an adsorbent. The longer the adsorption time, the more adsorbate adsorbed. Until a certain point, increasing the adsorption time did not increase the amount of adsorbate adsorbed significantly. At this point, the adsorbent is saturated, and all of the active sites on the adsorbent surface are already formed bonds with adsorbate molecules.

The adsorption time influences were investigated in pure gasoline, water, and gasoline from BA adsorption processes, and the adsorption capacities were calculated using Eq. 1.

The effect of increasing adsorption time on the adsorption capacity of pure gasoline is shown in Fig. 11. From Fig. 11 it can be seen that the process of gasoline adsorption has already begun at an adsorption time of 1 min. The highest adsorption capacity of pure gasoline was 1429 mg per g of adsorbent and it reached within 4 min.

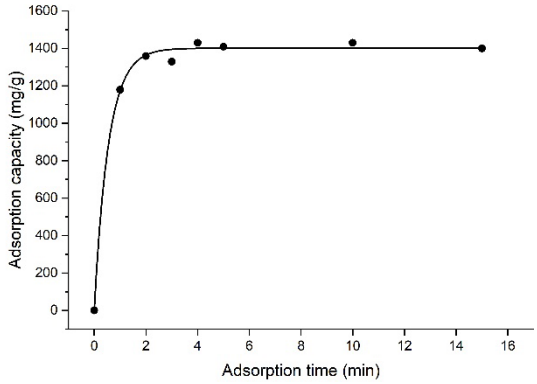

Fig. 11: The adsorption capacity of pure gasoline as increasing adsorption time

The highest point of the pure water adsorption was taken place at the adsorption time of 2 min, with an adsorption capacity of 1579 mg/g, as shown in Fig. 12. After 2 min, the adsorption capacity decreased and then it constant at about 1500 mg/g. Even though AC-M was confirmed as a hydrophobic adsorbent and gave a water contact angle close to 90 °, the surface of AC-M still adhered to water in the absence of gasoline[17].

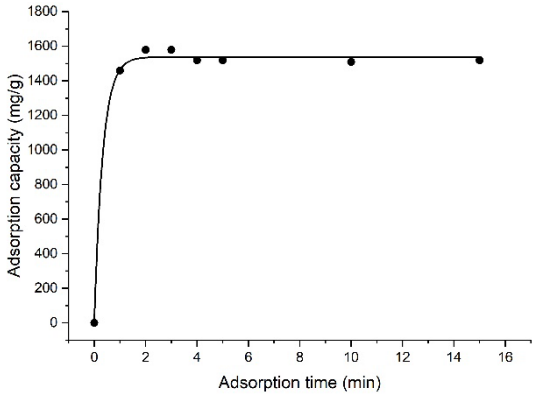

Fig. 12: The adsorption capacity of pure water as increasing adsorption time

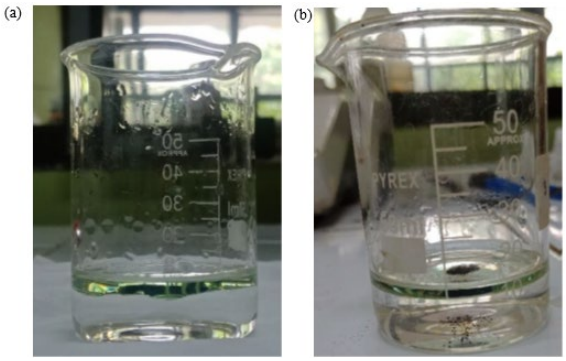

Fig. 13: (a) AC-M was placed on a gasoline layer, and (b) AC-M fell to the bottom of the water after some time

Fig. 13 shows the phenomenon that happened when the simulation of the gasoline adsorption process from water surfaces takes place. When AC-M was carefully placed on BA, an artificial oil spilled on water surfaces, all of the

AC-M particles were on the gasoline layer and were in contact with gasoline. After some time, some of the AC-M particles fell into the bottom of the water as shown in Fig. 13. The falling of AC-M powder denoted the adsorbent has already saturated with gasoline, which means all the active sites on the AC-M surface are already formed bonds with gasoline. Fig. 14 shows the adsorption capacity of gasoline from BA in increasing adsorption time. The highest adsorption capacity was 1560 mg/g and occurred at the adsorption time of 5 min.

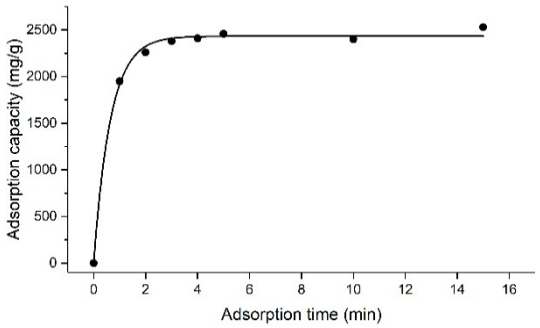

Fig. 14: The adsorption capacity of gasoline from BA as increasing adsorption time

3.3.2 The effect of adsorbent/adsorbate ratio

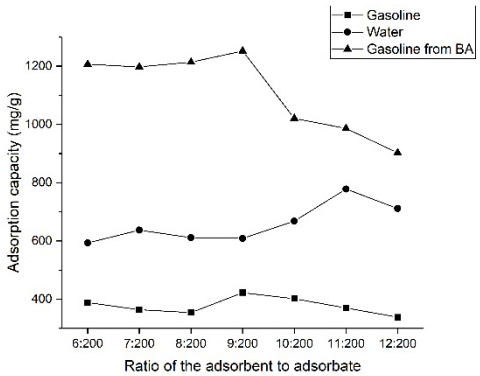

Fig. 15: The influence of the mass of adsorbent on the adsorption capacity of pure gasoline, pure water, and gasoline from the BA adsorption process

The influence of the adsorbent to adsorbate ratio on the adsorption capacity was shown in Fig. 15. The ratio of the adsorbent to adsorbate is another factor that affects adsorption capacity. It can determine the effectiveness and efficiency of the adsorbent in the adsorption process. Furthermore, knowing its effects on adsorption capacity can increase the cost-effectiveness because it can prevent waste in adsorbents used in the fields and how much the adsorbent is needed to adsorb all the oil spills. Fig. 15 shows the influence of the adsorbent to adsorbate ratio on adsorption capacity. As in the adsorption time influences observation, the adsorbent to adsorbate influences was investigated in pure gasoline, water, and gasoline from BA adsorption processes by AC-M adsorbent. All the adsorption tests were conducted in 4 min because the gasoline, the targeted adsorbate, adsorption process reached equilibrium at the adsorption time of 4 min. The adsorption capacities were calculated using Eq. 1.

From Fig. 15, it can be seen that the highest pure gasoline adsorption capacity was 422.22 mg/g occurred when the adsorbent vs adsorbate ratio was 9:200. The highest point of the pure water adsorption was when the adsorbent vs adsorbate ratio was 11:200 with an adsorption capacity of 778.18 mg/g. The highest adsorption capacity of gasoline from the BA adsorption process was 1252.22 mg/g when the adsorbent vs adsorbate ratio was 9:200.

3.3.3 Adsorption kinetics study

The study of adsorption kinetics results in the adsorption rate constant, the adsorbent's performance, and the mass transport mechanism[7]. The adsorption rate constant (k) is determined from the equation according to the adsorption kinetics model used to study the adsorption kinetics[20]. Several adsorption kinetics models are widely used to describe the performance of the adsorption process. In this work, the experimental data were investigated by the PFO model, PSO model, and IPD model.

The optimum experiment conditions are as follows; the adsorption time of 4 min and the adsorbent vs adsorbate ratio of 9:200. The plot graphs for all three models used to interpret the experimental data are shown in Fig. 16, and the corresponding kinetic parameters and correlation coefficients (R^2) are summarized in Table 3.

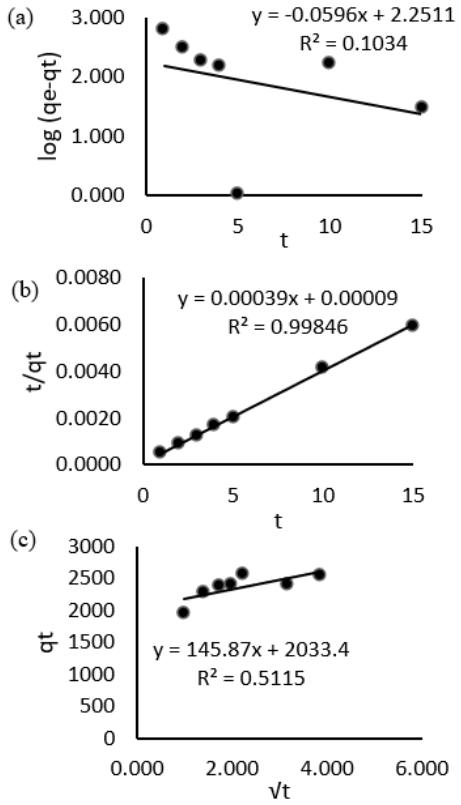

Fig. 16: Plot for (a) PFO kinetic model, (b) PSO kinetic model, and (c) IPD model for gasoline adsorption onto AC-M magnetic adsorbent

Table 3. Kinetic parameters of the PFO, PSO, and IPD kinetic models

Kinetic model	R^2	k	Unit of k
Pseudo-first-order	0.1034	0.137	min^{-1}
Pseudo-second-order	0.9985	0.0018	g/mg/min
Intra-particle diffusion	0.5115	145.87	$min^{-1/2}$

Fig. 16 shows the plot graphs for three kinetics models. Fig. 16(a) shows the plot graph for the pseudo-first-order model was made by plotting $\log(q_e - q_t)$ vs t. The linear equation for this model was $y = -0.0596x + 2.2511$ with the R^2 value of 0.1034. The R^2 value of this model is very low, indicating that this model does not fit to describe the adsorption process of gasoline from water surfaces using AC-M adsorbent.

Fig. 16(b) shows the graph of t/q_t vs t plotting that describes the pseudo-second-order model. The equation and R^2 value obtained from the graph were $y = 0.00039x + 0.00009$ and 0.99846. From the equation, the adsorption rate k is obtained, 0.0018 g/mg/min.

Fig. 16(c) shows the graph of q_t vs $\sqrt{t}$ that describes the intra-particle diffusion model. The IPD model was used to identify the gasoline diffusion mechanism onto the AC-M's surface[20]. The linearity of the plot for the IPD model is low with the R^2 value of 0.5115 and the graph did not cross the origin. This signifies that intra-particle diffusion is not the rate-determining step[20].

The best fit kinetic model was determined by the R^2 closest to 1[7]. Based on Table 3, the R^2 value for the PSO model is the highest and closest to 1 compared to the other models. Therefore, it can be concluded that the PSO kinetic model is the best fit to describe the adsorption process of gasoline from the gasoline-water mixture using AC-M adsorbent. The assumptions of this model are the adsorption process is in second order and the rate-limiting factor is chemisorption. The chemisorption process occurs through electron pairs exchange or sharing between the adsorbent and adsorbate. The adsorption rate is affected by the adsorption capacity and not by the concentration of the adsorbate.

4. Conclusion

The activated carbon-Fe_3O_4 composite has been successfully synthesized by microwave-assisted pyrolysis followed by co-precipitation methods. The composite has been confirmed as a hydrophobic adsorbent and thus has selectivity towards gasoline over water. This property was proved by the results of the contact angle analysis where water forms the most significant contact angle (84.156 ˚), followed by the gasoline-water mixture (72.928 ˚), and the latest is the gasoline which is directly absorbed without forming a contact angle (0 ˚). The activated carbon-Fe_3O_4 composite can be used as a promising magnetic adsorbent for gasoline from the water surface. The optimum adsorption conditions for the gasoline adsorption process were 4 min of adsorption time and the adsorbent vs adsorbate ratio of 9:200, with an adsorption capacity of 1252.22 mg/g. The process of gasoline adsorption follows the pseudo-second-order kinetic model from Ho and McKay with the R^2 value of 0.9985 and the rate constant (k) of 0.0018 g/mg/min.

Acknowledgments

The authors would like to thank the Chemistry Department of Gadjah Mada University for supporting this research.

Nomenclature

q_t	adsorption capacity at a given time (mg/g)
q_e	adsorption capacity at equilibrium (mg/g)
m_t	mass of adsorbed adsorbate (mg)
m_0	mass of adsorbent used (g)
k_1	adsorption rate constant of PFO kinetic model (min^{-1})
k_2	adsorption rate constant of PSO kinetic model (g/mg/min)
k_{id}	intra-particle diffusion rate constant
t	time (min)
R^2	correlation coefficient

References

1) K. Qiao, W. Tian, J., Bai, L. Wang, J. Zhao, Z. Du, and X. Gong, "Application of magnetic adsorbents based on iron oxide nanoparticles for oil spill remediation: a review," *J. Taiwan Inst. Chem. Eng.*, **97**, 227-236 (2019).
2) G. da Costa Cunha, N. C. Pinho, I. A. A. Silva, J. A. S. Costa, C. M. P. da Silva, and L. P. C. Ramão, "Removal of heavy crude oil from water surfaces using a magnetic inorganic-organic hybrid powder and membrane system," *J. Environ. Manage.*, **247**,9-18 (2019).
3) Z. Luo, X. Wang, D. Yang, S. Zhang, T. Zhao, L. Qin, and Z. Z. Yu, "Photothermal hierarchical carbon nanotube/reduced graphene oxide microspherical aerogels with radially orientated microchannels for efficient cleanup of crude oil spills," *J. Colloid Interface Sci.*, **570**, 61-71 (2020).
4) Z. Rahmani, M. Shafei-Alavijeh, A. Kazemi, and A.

M. Rashidi, "Synthesis of MIL-101@nanoporous graphene composites as hydrophobic adsorbents for oil removal," *J. Taiwan Inst. Chem. Eng.*, **91**, 597-608 (2018).
5) K. G. Raj, and P. A. Joy, Coconut shell based activated carbon-iron oxide magnetic nanocomposite for fast and efficient removal of oil spills," *J. Environ. Chem. Eng.*, **3**, 2068-2075 (2015).
6) A. K. Fard, G. Mckay, R. Chamoun, T. Rhadfi, H. Preud'Homme, and M. A. Atieh, "Barium removal from synthetic natural and produced water using MXene as two dimensional (2-D) nanosheet adsorbent," *Chem. Eng. J.*, **317**, 331-342 (2017).
7) M. Sharma, M. Joshi, S. Nigam, D. K. Avasthi, R. Adelung, S. K. Srivastava, and Y. K. Mishra, "Efficient oil removal from wastewater based on polymer-coated superhydrophobic tetrapodal magnetic nanocomposite adsorbent," *Appl. Mater. Today*, **17**, 130-141 (2019).
8) E. Reknosari, T. Wirawan, and S. Koesnarpadi, "Adsorpsi fenol menggunakan adsorben komposit Fe_3O_4-arang aktif ampas kopi," *Jurnal Kimia Mulawarman*, **18** (1), 30-37 (2020).
9) R. S. Juang, Y. C. Yei, C. S. Liao, K. S. Lin, H. C. Lu, S. F. Wang, and A. C. Sun, "Synthesis of magnetic Fe_3O_4/activated carbon nanocomposites with high surface area as recoverable adsorbents," *J. Taiwan Inst. Chem. Eng.,* **90**, 51-60 (2018).
10) A. F. Ridassepri, F. Rahmawati, K. R. Heliani, Chairunnisa, J. Miyawaki, dan A. T. Wijayanta, "Activated Carbon from Bagsse and its Application for Water Vapor Adsorption," *EVERGREEN*, **07** (3), 409-416 (2020).
11) N. Li, X. Ma, Q. Zha, K. Kim, Y. Chen, and C. Song, "Maximizing the number of oxygen-containing functional groups on activated carbon by using ammonium persulfate and improving the temperature-programmed desorption characterization of carbon surface chemistry," *CARBON*, **49**, 5002-5013 (2011).
12) Y. Wibisono, A. Amanah, A. Sukoyo, F. Anugroho, and E. Kurniati, "Activated Carbon Loaded Mixed Matrix Membranes Extracted from Oil Palm Empty Fruit Bunches for Vehicle Exhaust Gas Adsorbers," *EVERGREEN*, **08** (03), 593-600 (2021)
13) F. D. Kurniati, Pardoyo, and Suhartana, "Sintesis arang aktif dari tempurung kelapa dan aplikasinya untuk adsorpsi asap cair," *J. Kim. Sains Apl.*, **14** (3), 72-76 (2011).
14) M. J. Rampe, B. Setiaji, W. Trisunaryanti, and Triyono, "Fabrication and characterization of carbon composite from coconut shell carbon," *Indo. J. Chem.*, **11** (2), 124-130 (2011).
15) J. Georgin, G. L. Dotto, M. A. Mazutti, and E. L. Foletto, "Preparation of activated carbon from peanut shell by conventional pyrolysis and microwave irradiation-pyrolysis to remove organic dyes from aqueous solutions," *J. Environ. Chem. Eng.*, **4**, 266-275 (2016).
16) D. Nuryana, M. F. R. Alim, M. Yahayu, M. a. Ahmad, R. S. R. Sulong, M. F. S. Abd Aziz, H. Prasetiawan, Z. A. Zakaria, and R. D. Kusumaningtyas, " Methylene blue removal using coconut shell biochar synthesized through microwave-assisted pyrolysis," *Jurnal Teknologi*, **82** (5), 31-41 (2020).
17) A. Kozbial, C. Trouba, H. Liu, and L. Li, "Characterization of the intrinsic water wettability of graphite using contact angle measurements: effect of defects on static and dynamic contact angles," *Langmuir*, **33**, 959-967 (2017).
18) Z. Tang, D. W. Hess, and V. Breedveld, "Fabrication of oleophobic paper with tunable hydrophilicity by treatment with non-fluorinated chemicals," *J. Mater. Chem. A*, **3**, 14651-14660 (2015).
19) D. L. Williams, A. T. Kuhn, M. A. Amann, M. B. Hausinger, M. M. Konarik, and E. I. Nesselrode, "Computerized measurement of contact angles," *Galvanotechnik*, **101** (11), 2502-2512 (2010).
20) J. Wang, and X. Guo, "Adsorption kinetic models: Physical meanings, applications, and solving methods," *J. Hazard. Mater.*, **390**, 122156 (2020).
21) H. Yuh-San, "Citation review of Lagergren kinetic rate equation on adsorption reactions," *Scientometrics*, **59** (1), 171-177 (2004).
22) F. Jerai, B. B. Saha, T. Miyazaki, and S. Koyama, "Overview of adsorption cooling system based on activated carbon-alcohol pair," *EVERGREEN*, **02** (01), 30-40 (2015).
23) B.H. Toby and R.B. Von Dreele, " GSAS-II: the genesis of a modern open-source all purpose crystallography software package," *J. Appl. Cryst.*, **46**, 544-549 (2013).
24) B. A. Wechsler, D. H. Lindsley, and C. T. Prewitt, "Crystal structure and cation distribution in titanomagnetites ($Fe_{3-x}Ti_xO_4$)," *American Mineralogist*, **69**, 754-770 (1984).
25) J. Miyawaki, J. Yeh, H. S. Kil, J. K. Lee, K. Nakabayashi, I. Mochida, and S. H. Yoon, "Influence of pore size and surface functionality of activated carbons on adsorption behaviors of indole and amylase," *EVERGREEN*, **03** (02), 17-24 (2016).
26) R. N. P. Teixeira, V. O. S. Neto, J. T. Oliveira, T. C. Oliveira, D. Q. Melo, M. A. A. Silva, and R. F. Nascimento, "Study of the use of Roasted Barley Powder for Adsorption of Cu^{2+} Ions in Batch Experiments and in Fixed-bed Columns," *BioResources*, **8** (3), 3556-3573 (2013).
27) M. Thommes, K. Kaneko, A. Neimark, J. Olivier, F. Rodriguez-Reinoso, J. Rouquerol, and K. Sing, "Physisorption of gases, with special reference to the evaluation of surface area and pore size distribution (IUPAC Technical Report)," *Pure Appl. Chem.*, **87** (9-10), 1051-1069 (2015).